Journal of Earth Science, *Vol. 28*, *No. 1*, *p. 180–186*, *February 2017* *ISSN 1674-487X*
Printed in China
DOI: 10.1007/s12583-017-0741-9

Hydrocode Simulation of the Impact Melt Layer Distribution underneath Xiuyan Crater, China

Zongyu Yue*, Kaichang Di
State Key Laboratory of Remote Sensing Science, *Institute of Remote Sensing and Digital Earth*, *Chinese Academy of Sciences*, *Beijing* 100101, *China*
Zongyu Yue: http://orcid-org/0000-0002-8073-9264

ABSTRACT: In this research, we studied the distribution of impact melt layers underneath Xiuyan crater using hydrocode simulation. The target was modeled by granite based on the rock type distribution around the crater and projector by iron, because most small and isolated terrestrial craters are formed by iron projectile. The simulated crater diameter and depth are 1 710 and 320 m, respectively, which are in good agreement with observations of 1 800 and 307 m (except for the post-impact lacustrine sedimentation). The validated model shows that impact melt materials were first formed along the transient crater floor and wall by highshock pressure, and then refilled inward the crater along with collapse of the crater wall. The final style of impact melt materials is interbedded with shock breccia underneath the crater center, which is verified through two layers in the borehole located in the crater center.
KEY WORDS: Xiuyan crater, numerical simulation, impact melt.

0 INTRODUCTION

Xiuyan crater is located at 40.37°N, 123.46°E in the Liaodong Peninsula, and its impact origination was confirmed through investigation of shock effects on rocks and minerals, such as planar deformation features (PDFs) in quartz and shock-induced high-pressure polymorph transition (Chen, 2008). The diameter of the crater is approximately 1.8 km, and the rim is about 200 m higher than the floor. The crater had been moderately weathered, which is evident from the overlaid lacustrine sediments. Chen (2008) drilled a borehole of 307 m close to the crater center, through which its original appearance can be roughly reconstructed. Underneath 107 m of lacustrine sediments, hornblendite and a small amount of melt-bearing polymict breccia were found. Therefore, the crater should have a depth of about 307 m when it was originally formed and is then classified as a simple crater based on its scale.

At the bottom of the borehole stratigraphy from 295 to 307 m, fractured tremolite was found and considered to be the fractured bedrock (Chen et al., 2010). Notably, melt-bearing materials are found at both the top and the bottom of the drilled column (except for the lacustrine sediments and the fractured bedrock, Chen et al., 2010), and other shock fragments were sealed inside the drilled column. In impact cratering, melting occurs at locations in both the projectile and the target, in which the peak shock pressure exceeds the value required for complete melting. An isobaric core with extremely high shock pressure was generally believed to exist at the center of the transient impact craters, and shock pressure and particle velocity decays exponentially outside the center (Tonks and Melosh, 1993). As a result, the impact melt material is concentrated in the transient crater center. However, the transient crater is greatly modified at the late stage, and thus the impact melt materials are translocated. For small craters like Xiuyan crater, the melt materials are stratified and jagged with shock breccia.

A similar distribution of impact melt layers has also occurred in Brent crater, which is a simple crater located 46.08°N, 78.48°W with an original diameter of 3.8 km. The borehole located at the crater center intersected both the melt-bearing mixed breccia of the upper portion of the breccia lens and the basal melt-zone (Grieve, 1978). Therefore, establishing impact melt layer distribution that is similar to those of other small craters is beneficial, and Xiuyan and Brent craters are two specific examples. And illustrating the mechanism of such phenomenon in small craters, which is also instructive in selecting the location of boreholes to determine new small craters, seems urgently needed.

However, to the best of our knowledge, no research particularly aimed to illustrate the mechanism of impact melt layer distribution in simple craters has been published. For the Xiuyan crater, Wang et al. (2013) gave an estimate of the morphological features of the Xiuyan crater using several empirical relations, which would provide basic information on the formation of the crater. However, a more extensive study on the crater through numerical simulation, which can present the formation process of the crater, determine all thermodynamic parameters in each time step, and then reveal the latent mechanisms of many observations, has not been conducted. This

*Corresponding author: yuezy@radi.ac.cn

Manuscript received December 29, 2014.
Manuscript accepted January 22, 2015.

paper aims to characterize the impact melt layer formation and evolution of Xiuyan crater through numerical simulation. Results of this study may also apply to other simple craters of a similar order on the Earth.

1 FORMATION OF XIUYAN CRATER AND IMPACT MELT

1.1 Geologic Background of Xiuyan Crater

Xiuyan crater is located in the Early Proterozoic crystalline basement (Chen et al., 2011). Two other small areas of rocks, which are mainly composed of Jurassic basalt and Yanshanian granites, are located at about 2 500 m east and the west limb of the crater, respectively. The rock types in a wider area surrounding Xiuyan crater are composed of a Proterozoic metamorphic rock complex, which include leptynites, amphibolites, tremolite, gneisses, and marbles (Chen et al., 2010). Logically, the Proterozoic crystalline basement is the target area when the crater is formed.

The stratigraphic column from the borehole can also provide information on geologic background. In the depth interval from 107 to 260 m, unconsolidated fragments of the crystalline basement with fine-grained clasts and sands were encountered, which consist mainly of granulite, hornblendite, gneiss, and tremolite marble. These fragments are the refilled materials in the modification stage of the cratering process and can thus represent the target rocks. The rock types inside the borehole are similar to those in the surrounding crater, which justifies the validity of considering the Proterozoic crystalline basement as target rocks.

1.2 Formation of Xiuyan Crater

As a typical simple crater, Xiuyan crater was formed in three stages: compression, excavation, and modification (Melosh, 1989). The compression stage begins with the contact between the projectile and the target, which occurred about 50 000 years ago in Xiuyan crater based on isotope analysis of sediments inside the crater. After the projectile impacted the target, a shock wave was generated in the contact point(s). The shock wave spherically expands from the contact point(s) to both the target and the projectile, and the strength of the shock wave rapidly attenuates when propagating both for energy loss and energy density decrease. The shock wave presents a hemispherical shape, and its size is comparable to the projectile diameter (Melosh, 1989). Therefore, the center of the crater is generally considered as a region with extremely high shock pressure. For Xiuyan crater, the region currently experiences a pressure of more than 20 GPa, which is derived from the predominant orientations of PDFs (Grieve et al., 1996), or more than 30 GPa from the occurrence of coesite (Chen et al., 2011). Notably, this pressure is not necessarily the maximum peak shock pressure in the impact process. However, this value can provide a lower boundary of the shock pressure in the simulation. The generated shock pressure has evidently exceeded the Hugoniot elastic limit of the material, and the targets were plastically deformed, melted, metamorphosed by phase change, or even vaporized. As a result, a large fraction of the initial kinetic energy is converted to internal energy in the region of impact. The shock wave propagating in the projectile will be reflected back when upon reaching the rear point (i.e., point antipodal to the contact point), and the resulting rarefaction wave will unload the compressed projectile. The rarefaction wave will propagate to the front at a higher velocity than the previous shock wave. When the entire projectile is released from high pressure, the compression stage is terminated (Melosh, 1989).

At the end of the compression stage, rarefaction will still further propagate into the target through the impact boundary. The transmitted rarefaction wave will unload the compressed target, which makes the target obtain a velocity with an inverse direction compared with that in the compression stage. Given the irreversibility of the shock compression process, the vector sum of the two velocities will have the same direction, with the velocity in the compression stage and the material being spurted out in the form of an ejecta curtain. Outside the Xiuyan crater, Qin et al. (2001) found many breccia rocks, which are probably formed in this process. This process marks the excavation stage, and a transient crater with a diameter of 1 406±12 m and depth of 497±4 m was derived for the Xiuyan crater (Wang et al., 2013).

In the modification stage, loose material from the impact slumps inward to the crater, which makes the crater shallow. The material is mainly controlled by planetary gravity acceleration where the crater is located. Collapse morphologies strongly depend on the size of the craters and gravity. Large craters typically collapse considerably more spectacularly than small ones, and thus their final morphologies widely vary. In simple craters like the Xiuyan crater, the collapse mostly involves debris flow and is floored by a lens of breccia, which includes the impact melt formed during the previous stages. From the analysis of the seismic wave within the crater, an unconsolidated layer of greater than 100 m existed, resulting from modification (Zhao et al., 2011).

1.3 Impact Melt Formation

The thermodynamic state of one material can usually be determined by any three variables (e.g., pressure, temperature, and volume), by which we can judge if the material has melted or vaporized. However, if a kind of constrained relation existed between these thermodynamic variables, any two parameters can be used to determine the material state. In the impact process, the target is first compressed by the shock wave following the Hugoniot curve, and then released by rarefaction wave along an isentropic path (Melosh, 1989). The image in Fig. 1 shows a typical thermodynamic path of the target material in the impact process, in which the material is first compressed to point *a* in Hugoniot curve (the state jumps to point a discontinuity) and then released along the vertical line. In the process, the material first exists in a solid state, will be melted when the vertical line intersects with the melt curves (the two broken lines of *I* and *C* denote incipient and complete melt, respectively) and partial vaporization would occur because of the decrease in melting point with the reduced pressure. In the figure, a critical point (*CP*) divides the region of solid and dissociated vapor, at which the material would directly sublimate from solid and then become liquid and finally vapor. Therefore, to determine whether most materials have melted in

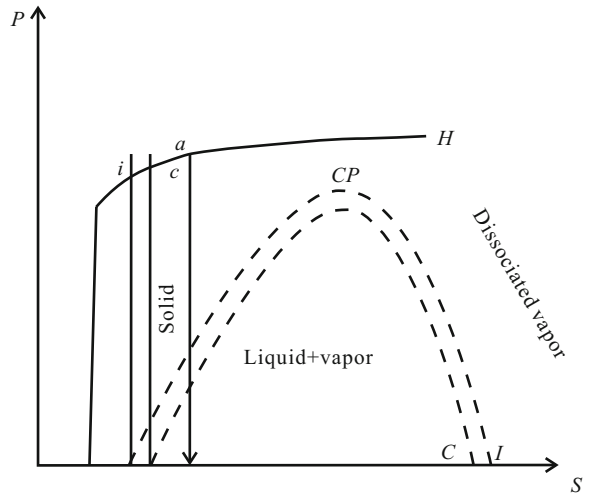

Figure 1. Diagram of the Hugoniot and melt curves. The solid line *H* denotes the Hugoniot curve of the target material upon impact, and the two dashed lines *I* and *C* indicate the incipient and complete melt lines of the material, respectively. Upon impact, the state of the target material jumped to *a* in the Hugoniot curve and is then released along an isentropic line. Curves *i* and *c* indicate that the target material will be melted incipiently and completely according to their intersections with melt curves. See context for details.

the impact process, two important points signify the minimum shock pressure for incipient (point *i*) and complete melting (point *c*). In the numerical simulation of impact craters, we can determine whether the target materials have melted by checking if their peak pressures exceeded the threshold values. For granite, the incipient and complete melting pressures are 46 and 56 GPa, respectively (Pierazzo et al., 1997). Notably, the Hugoniot curve is related with the material's initial state, and then the melting pressures are also affected by the initial state, although only to a small extent. The initial-state density, temperature, and pressure for deriving the above values are 2.63 g/cm^3, 298 K, and 0 Pa, respectively (Pierazzo et al., 1997), which are applicable in our research.

Impact melt occurs in numerous different forms, including melt spherules and breccias. Spherules most likely result from the vapor, whereas breccias result from the melt. Therefore, these forms can be used to indicate different shock pressures (Osinski and Pierazzo, 2013). Shock pressure is determined by the material equation of state (EoS) and the initial impact conditions, and can be solved analytically and/or numerically through the conservation of mass, momentum, and energy, along with the EoS. In addition, the occurrence of impact melt is also an indicator of the impact velocity and is therefore important in the study of crater formation.

2 HYDROCODE MODELING

Considerable effort has been devoted to development of computer codes because of the importance of numerical simulation in the study of impact cratering process (for example, the CTH code, McGlaun et al., 1990). In this research, we used iSALE2D (Wünnemann et al., 2006), which was developed on the basis of the SALE hydrocode (Amsden et al., 1980). The code was improved to include an elasto-plastic constitutive model, fragmentation models, various EoSs, and multiple materials (Ivanov et al., 1997; Melosh et al., 1992). A modified strength model (Collins et al., 2004) and a porosity compaction model (Wünnemann et al., 2006) have recently been included. All mechanic models, Newton's laws of motion, and EoS constitute the physical principles behind the computer code (Melosh, 2007). Therefore, we will provide a thorough description of these models and list the corresponding parameters for Xiuyan crater simulation.

2.1 EoS of the Target and the Projectile

The rock types in a wide area surrounding the crater are composed of Proterozoic metamorphic rocks, including granulite, hornblendite, gneiss, tremolite marble, and marble (Chen et al., 2011), which shows that the target area is inhomogeneous in composition. Although including all of the above rock types into the hydrocode simulation is preferable, accomplishing such a task is virtually impossible, mostly because of the absence of the EoS for these rocks, especially under extremely high pressure and temperature. A general treatment in crater simulation involves simplifying the stratum with the primary component (e.g., Littlefield et al., 2007; Pierazzo and Melosh, 2000). Considering that the target material of Xiuyan crater pre-impact is mostly composed of Proterozoic crystalline, the target material is then simplified as granite in the hydrocode simulation, and such simplification is also used for the simulation of other terrestrial craters. For example, Ivanov and Artemieva (2011) also used granite to represent the target material of Popigai crater, in which layers of Archean gneisses covered with an inhomogeneous sedimentary and metasedimentary rock system existed.

For isolated small craters with diameters less than 2.5 km in the earth surface, most of the projectiles are composed of iron (Osinski and Pierazzo, 2013). This composition is because the iron meteoroid projectile is strong enough to withstand crushing from the atmosphere, while the stony projectile could be possibly destroyed, and a resulting crater field would be formed on the earth surface (Melosh, 1989). Although PGE anomaly and the existence of platina have been observed around Xiuyan crater (Qin et al., 2001), the primary composition of the projectile remains incompletely defined at present, and the projectile is also considered as an iron meteorite in the research.

The above treatments applied to target and projectile materials seem arbitrary. However, concerns regarding the set-up are unfounded, because upon the hypervelocity impact, the strength of these materials has been obscured by the extremely high shock pressure, although the strength may become important when the strength of the shock wave weakens. This research is aimed to interprete the formation and distribution of impact melt distribution, which is closely related with the pattern of shock pressure in the impact. Thus, the composition of materials should not exert a major effect on our conclusion, because the patterns of shock pressure are similar for different materials, as proven by physical experiments (Kinslow, 1970). Therefore, the derived distribution of impact melt should not be considerably affected by our selection of materials in this research.

Several categories of EoS currently describe the state of materials under shock pressure (Melosh, 1989). In this research, we used a kind of analytical EoS (ANEOS) to calculate the thermodynamic state of granite and iron (Thompson and Lauson, 1972), because the EoS includes a series of analytical expressions to describe the thermodynamic state surface (Littlefield, 1997; Melosh, 1989). The ANEOS was coded in FORTRAN programming language, and extensive input parameters must be provided to obtain the results (Thompson and Lauson, 1972). The iron ANEOS parameters are included in the code, whereas the parameters of granite can be referenced to Pierazzo et al. (1997).

2.2 Mechanical Models

The mechanical models in the hydrocode are used to describe material mechanical response to external deviator stress. These models are also extremely important in numerical modeling, because these models predict material deformation under the external force. In addition, the results of the laboratory experiments cannot be simply extrapolated to the scale of a natural impact, which also renders the mechanical models critical to the success of the simulation. In general, the more comprehensive the models means that more accurate results will be derived. In this research, we used the IVANOV of damage model, ROCK of the strength model, and the OHNAKA of the thermal softening model to simulate the mechanical properties of the materials. Yue et al. (2012) provided a short description of the above models, and the corresponding parameters with their descriptions are listed in Table 1.

2.3 Mesh Properties

In the research, we first used scaling laws to estimate projectile diameters and duration time (Collins et al., 2005), and multiple models were then tested. In the best-fit model, the diameter of the projectile was 100 m, and the impact velocity was 17.0 km/s, which was the average impact velocity. Moreover, this velocity is sufficient to produce impact melt and vapor (O'Keefe and Ahrens, 1994).

In the simulation, we adopted cylindrical symmetry method to describe the target area. The impact point is located atthe center of the cylinder surface, and the projector center is situated on the vertical axis. The target material is under the projectile, and extends both horizontally and vertically to a distance far enough to reduce the effect of the reflected shock wave. To obtain a precise result while reducing the amount of calculation, only the center of the cylinder is set with a high resolution of 10 m, whereas the other regions are exaggerated at a factor of 1.05 times their previous cells, and a maximum exaggeration factor of 20 is set to the high resolution. The crater is completely represented in high resolution.

We set the tracers from the target surface down deep in high resolution, in which the state of the meshes can be tracked at each time step, and we can quantitatively analyze the impact melt material formation and evolvement with crater formation. Mesh parameters are listed in the following table.

Table 1 Parameters for mechanical models used in the research

Models	Parameters	Description	Target	Projectile
IVANOV of damage model (Collins et al., 2004)	ϵ_{fb}	Minimum failure strain for low pressure states	10^{-4}	10^{-4}
	B (Pa^{-1})	Positive constant	10^{-11}	10^{-11}
	p_c (MPa)	Pressure above which failure is always compressional	300.0	300.0
ROCK of strength model (Wünnemann et al., 2008)	Y_{d0} (KPa)	Cohesion of damaged material at zero pressure	10.0	0.01
	μ_d	Coefficient of internal friction for damaged material	0.6	0.4
	Y_{dm} (GPa)	Limiting strength at high pressure for damaged material	2.5	1.7
	Y_{i0} (MPa)	Cohesion of intact material	10.0	5.0
	μ_i	Coefficient of internal friction for intact material	2.0	1.0
	Y_{im} (GPa)	Limiting strength at high pressure for intact material	2.5	1.7
OHNAKA of thermal softening model (Ohnaka, 1995; Wünnemann et al., 2008)	T_{m0} (K)	Melt temperature at zero pressure	1 673.0	1 811.0
	a (GPa)	Constant in Simon approximation	6.0	6.0
	c	Exponent in Simon approximation	3.0	3.0
	ξ	Constant in thermal softening law	1.2	1.2

Table 2 Parameters for the mesh used in the research

Parameters	Values
Horizontal number cells from the left	0 : 150 : 200
Vertical number cells from the bottom	250 : 200 : 50
Extended factor	1.05
Grid spacing in high resolution	10 m
Maximum grid spacing factor	20
Tracer numbers from target surface	100 : 150

3 RESULTS

The formation and distribution of impact melt materials are closely related with crater formation, which is also the criterion for the success of our simulation. Therefore, we first show the results of the crater simulation and then analyze the formation of impact melt in the corresponding times.

3.1 Crater Formation

The Xiuyan crater simulation provides us with an insight into the formation process. At 1 s after contact, the target is

heavily compressed and excavated, as seen from Fig. 2a. This model predicts that the transient diameter is 1 510 m with a maximum depth of 550 m when the run time is 9 s (Fig. 2b). At this time, the crater has been excavated at its maximum, and we can see that the layers in the upper crater wall are overturned and the crater floor is heavily compressed. Afterwards, avalanches occur from the wall to the floor, and the accumulated material is piled up at the center of the crater floor, as seen from Fig. 2c at 20 s. As a simple crater with relatively lower energy, the center peak soon flattens down and cannot be stirred up again because of energy dissipation. Finally, the simulated crater shows a diameter of 1 710 m, with the depth of 320 m at 50 s (Fig. 2d). At this time, no further modification of the crater morphology occurs. The measured Xiuyan crater has a rim-to-rim diameter of about 1 800 m and a depth of 307 m, at which the fractured tremolite marble appeared (Chen et al., 2010). Taking weathering into consideration, the simulated result is in good agreement with the observation.

Our simulation is consistent with the borehole column both in composition and depth from the crater floor to the fractured bedrock. In the simulation, the depth between the transient and the final crater floor includes the slump from the crater wall, which is also the case in the borehole (Chen et al., 2010).

3.2 Impact Melt Material Distribution

Granite will completely melt at the shock pressure of 56 GPa (Pierazzo et al., 1997), and the impact melt material distribution can be studied through shock pressure. In our simulation, the melted material is approximately 0.18% in total of the traced mass. The image in Fig. 2 also shows the impact melt material (in red) distribution and its evolvement with time corresponding to 1, 9, 20, and 50 s. Immediately after contact, the impact melt materials were confined along the crater's inner wall (Fig. 2a). The impact melt material will stay along the surface until the time of the maximum excavation depth (Fig. 2b), during which the impact melt materials are ejected away along the crater surface. Then, the material in the crater's inner wall will slump down with the impact melt material layer (Fig. 2c), and impact material layers will overlap in certain regions. At the final stage, the impact melt material layer concentrates underneath the central crater and is distributed in several layers. Notably, some of the ejected melt material was distributed far away.

Underneath the central crater, two layers of impact melt are distributed as confirmed by the borehole. In addition, the simulation predicts multiple layers of impact melt, which needs further confirmation.

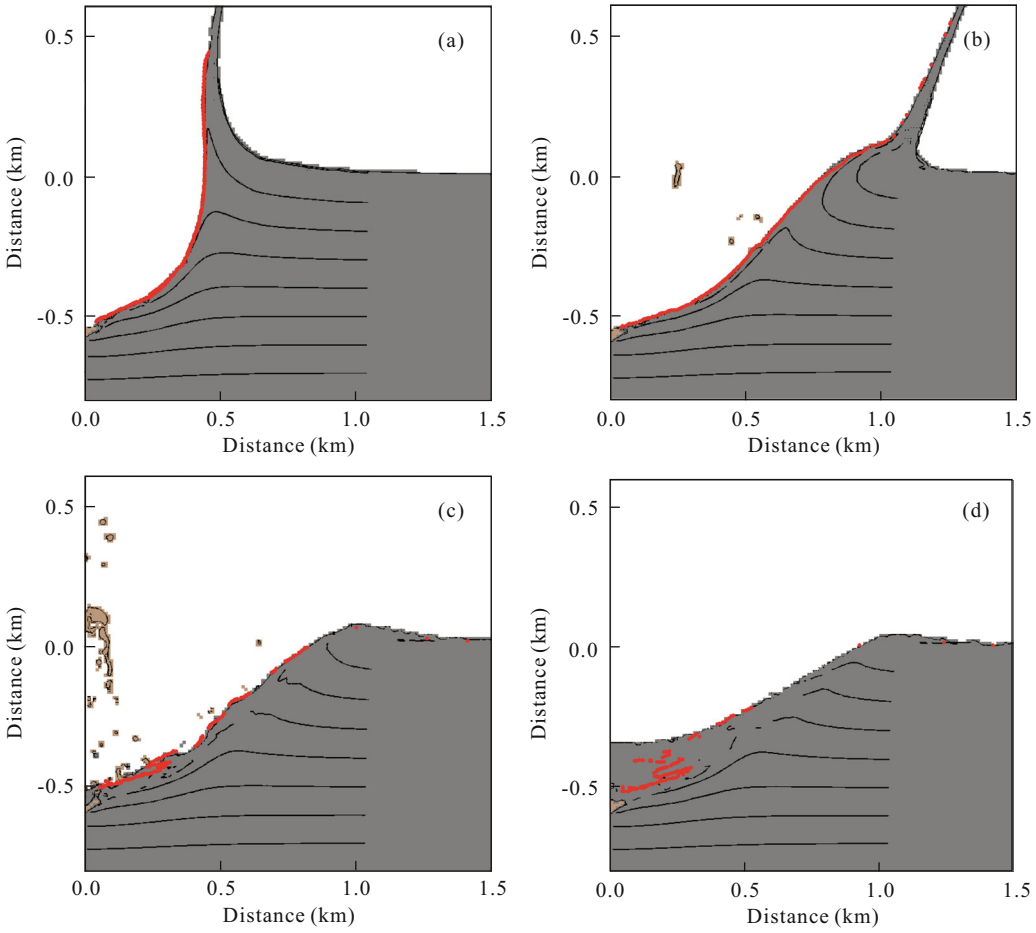

Figure 2. Crater formation simulation at 1 (a), 9 (b), 20 (c), and 50 s (d). The crater was opened after contact and compression (a), and continued to excavate until the transient crater is formed (b). Afterwards, the fragments from crater wall would slump inward the center (c) and finally shaped the crater (d). All scales are in km.

4 CONCLUSION AND DISCUSSION

In this paper, we present the best-fitting simulated results for the formation of the Xiuyan crater, which is consistent with the crater morphology and shock pressure. Based on the model, we studied the distribution of impact melt material layers, as shown in the borehole column. As shown in the simulation, the impact melt material initially lines the crater's inner wall and then slumps inward toward the crater center to form two layers at the top and bottom of the fragments. Our simulation is in good agreement with observations and can also be used to predict multiple layers of impact melt in some local areas.

The simulation of formation and dynamic evolution of impact melt over time presents considerable geologic implications for simple craters. For example, given that only small amount of impact melts occur in simple caters and they are originally distributed in a thin layer along the crater inner wall, the occurrence of the lowermost layer indicates the depth that crater has reached. Simultaneously, the topmost layer marks the surface of the collapse, and each layer overlays the original underneath layers. Therefore, the impact melt layers can be used to delineate the modification stage in a simple crater. In addition, the study of impact melt layer distribution can be used as guide to determine the impact origin of craters. Ejection also carries the impact melt, but only at a low amount and probably far away from the crater. Thus, finding the impact melt in ejection is difficult.

Given that we simulated the Xiuyan crater formation with a two-dimensional hydrocode, the impact angle is vertical to the surface. In fact, the most probable impact angle is 45°, and extremely few vertical impacts occur on a planet surface. However, although the impact angle may exert an important influence on the ejecta, the angle is weakly associated with impact melt layer distribution, because most of the transient craters are cone-shaped, except at extremely low incipient angles. In addition, impact melt layers are mostly related with gravity-dominated collapse.

ACKNOWLEDGMENTS

Part of this work was finished at Purdue University, and the first author appreciates the help by Prof. Jay Melosh. The authors acknowledge the developers of iSALE2D, including Gareth Collins, Kai Wünnemann, Boris Ivanov, Jay Melosh, and Dirk Elbeshausen. This study was supported by the National Natural Science Foundation of China (Nos. 41472303, 41490635). The final publication is available at Springer via http://dx.doi.org/10.1007/s12583-017-0741-9.

REFERENCES CITED

Amsden, A. A., Ruppel, H. M., Hirt, C. W., 1980. SALE: A Simplified ALE Computer Program for Fluid Flow at All Speeds. Report #LA-8095. Los Alamos National Laboratories, Los Alamos, New Mexico. 101

Chen, M., 2008. Impact-Derived Features of the Xiuyan Meteorite Crater. *Chinese Science Bulletin*, 53(3): 392–395. doi:10.1007/s11434-008-0004-3

Chen, M., Xiao, W. S., Xie, X. D., et al., 2010. Xiuyan Crater, China: Impact Origin Confirmed. *Chinese Science Bulletin*, 55(17): 1777–1781. doi:10.1007/s11434-010-3010-1

Chen, M., Koeberl, C., Xiao, W. S., et al., 2011. Planar Deformation Features in Quartz from Impact-Produced Polymict Breccia of the Xiuyan Crater, China. *Meteoritics & Planetary Science*, 46(5): 729–736. doi:10.1111/j.1945-5100.2011.01186.x

Collins, G. S., Melosh, H. J., Ivanov, B. A., 2004. Modeling Damage and Deformation in Impact Simulations. *Meteoritics & Planetary Science*, 39(2): 217–231. doi:10.1111/j.1945-5100.2004.tb00337.x

Collins, G. S., Melosh, H. J., Marcus, R. A., 2005. Earth Impact Effects Program: A Web-Based Computer Program for Calculating the Regional Environmental Consequences of a Meteoroid Impact on Earth. *Meteoritics & Planetary Science*, 40(6): 817–840. doi:10.1111/j.1945-5100.2005.tb00157.x

Grieve, R. A. F., 1978. The Melt Rocks at Brent Crater, Ontario, Canada. Proceeding of 9th Lunar Planetary Science Conference, March 13–17, Houston. 2579–2608

Grieve, R. A. F., Langenhorst, F., Stöffler, D., 1996. Shock Metamorphism of Quartz in Nature and Experiment: II. Significance in Geoscience. *Meteoritics & Planetary Science*, 31(1): 6–35. doi:10.1111/j.1945-5100.1996.tb02049.x

Ivanov, B. A., Deniem, D., Neukum, G., 1997. Implementation of Dynamic Strength Models into 2D Hydrocodes: Applications for Atmospheric Breakup and Impact Cratering. *International Journal of Impact Engineering*, 20(1–5): 411–430. doi:10.1016/s0734-743x(97)87511-2

Ivanov, B. A., Artemieva, N. A., 2011. Numerical Modeling of the Formation of Large Impact Craters. *Geological Society of America Special Paper*, 356: 619–630

Kinslow, R., 1970. High-Velocity Impact Phenomena. Academic Press, New York

Littlefield, D. L., 1997. ANEOS Extensions for Modeling Hypervelocity Impact. *International Journal of Impact Engineering*, 20(6–10): 533–544. doi:10.1016/s0734-743x(97)87442-8

Littlefield, D. L., Bauman, P. T., Molineux, A., 2007. Analysis of Formation of the Odessa Crater. *International Journal of Impact Engineering*, 34(12): 1953–1961. doi:10.1016/j.ijimpeng.2006.12.005

McGlaun, J. M., Thompson, S. L., Elrick, M. G., 1990. CTH: A Three-Dimensional Shock Wave Physics Code. *International Journal of Impact Engineering*, 10(1–4): 351–360. doi:10.1016/0734-743x(90)90071-3

Melosh, H. J., 1989. Impact Cratering: A Geologic Process. Oxford University Press, New York

Melosh, H. J., 2007. A Hydrocode Equation of State for SiO_2. *Meteoritics & Planetary Science*, 42(12): 2079–2098. doi:10.1111/j.1945-5100.2007.tb01009.x

Melosh, H. J., Ryan, E. V., Asphaug, E., 1992. Dynamic Fragmentation in Impacts: Hydrocode Simulation of Laboratory Impacts. *Journal of Geophysical Research*, 97(E9): 14735. doi:10.1029/92je01632

Ohnaka, M., 1995. A Shear Failure Strength Law of Rock in the Brittle-Plastic Transition Regime. *Geophysical Research Letters*, 22(1): 25–28. doi:10.1029/94gl02791

O'Keefe, J. D., Ahrens, T. J., 1994. Impact-Induced Melting of

Planetary Surfaces. *Geological Society of America Special Paper*, 293: 103–109

Osinski, G. R., Pierazzo, E., 2013. Impact Cratering: Processes and Products. Wiley-Blackwell, Hoboken, NJ

Pierazzo, E., Vickery, A. M., Melosh, H. J., 1997. A Reevaluation of Impact Melt Production. *Icarus*, 127(2): 408–423. doi:10.1006/icar.1997.5713

Pierazzo, E., Melosh, H. J., 2000. Melt Production in Oblique Impacts. *Icarus*, 145(1): 252–261. doi:10.1006/icar.1999.6332

Qin, G., Lu, D., Ou, Q., et al., 2001. The Discovery of PGE Anomaly and Platina from Luoquanli Impact Crater, China. *Earth Science Frontier*, 8(2): 333–338 (in Chinese with English Abstract)

Thompson S. L., Lauson, H. S., 1972. Improvements in the Chart D Radiation-Hydrodynamic CODE III: Revised Analytic Equations of State. Report SC-RR-71 0714. Sandia National Laboratory, Albuquerque. 119

Tonks, W. B., Melosh, H. J., 1993. Magma Ocean Formation Due to Giant Impacts. *Journal of Geophysical Research*, 98(E3): 5319. doi:10.1029/92je02726

Wang X. Y., Luo, L., Guo H. D., et al., 2013. Cratering Process and Morphological Features of the Xiuyan Impact Crater in Northeast China. *Science China*: *Earth Sciences*, 56(10): 1629–1638. doi:10.1007/s11430-013-4695-1

Wünnemann, K., Collins, G. S., Melosh, H. J., 2006. A Strain-Based Porosity Model for Use in Hydrocode Simulations of Impacts and Implications for Transient Crater Growth in Porous Targets. *Icarus*, 180(2): 514–527. doi:10.1016/j.icarus.2005.10.013

Wünnemann, K., Collins, G. S., Osinski, G. R., 2008. Numerical Modelling of Impact Melt Production in Porous Rocks. *Earth and Planetary Science Letters*, 269(3/4): 530–539. doi:10.1016/j.epsl.2008.03.007

Yue, Z. Y., Di, K. C., Zhang, P., 2012. Theories and Methods for Numerical Simulation of Impact Crater Formation. *Earth Science Frontiers*, 19(6): 110–117 (in Chinese with English Abstract)

Zhao, C. J., Liu, M. J., Fan, J. C., et al., 2011. High-Resolution Seismic Exploration of Xiuyan Impact Crater Structures. *Chinese Journal of Geophysics*, 54(6): 1559–1565 (in Chinese with English Abstract)